nature communications

Article

https://doi.org/10.1038/s41467-023-35986-3

Phonon-mediated room-temperature quantum Hall transport in graphene

Received: 26 November 2021

Accepted: 10 January 2023

Published online: 19 January 2023

Check for updates

Daniel Vaquero[1,10], Vito Clericò[1,10], Michael Schmitz[2,3], Juan Antonio Delgado-Notario[1,4], Adrian Martín-Ramos[1], Juan Salvador-Sánchez[1], Claudius S. A. Müller[5,6], Km Rubi[5,6], Kenji Watanabe[7], Takashi Taniguchi[8], Bernd Beschoten[2], Christoph Stampfer[2,3], Enrique Diez[1], Mikhail I. Katsnelson[6], Uli Zeitler[5,6], Steffen Wiedmann[5,6] & Sergio Pezzini[9] ✉

The quantum Hall (QH) effect in two-dimensional electron systems (2DESs) is conventionally observed at liquid-helium temperatures, where lattice vibrations are strongly suppressed and bulk carrier scattering is dominated by disorder. However, due to large Landau level (LL) separation (~2000 K at $B = 30$ T), graphene can support the QH effect up to room temperature (RT), concomitant with a non-negligible population of acoustic phonons with a wave-vector commensurate to the inverse electronic magnetic length. Here, we demonstrate that graphene encapsulated in hexagonal boron nitride (hBN) realizes a novel transport regime, where dissipation in the QH phase is governed predominantly by electron-phonon scattering. Investigating thermally-activated transport at filling factor 2 up to RT in an ensemble of back-gated devices, we show that the high B-field behaviour correlates with their zero B-field transport mobility. By this means, we extend the well-accepted notion of phonon-limited resistivity in ultra-clean graphene to a hitherto unexplored high-field realm.

Van der Waals heterostructures of graphene and hBN have recently granted experimental access to novel phenomena in condensed matter[1]. The use of hBN as atomically-flat encapsulating dielectric, in particular, permits a drastic reduction of extrinsic disorder in graphene devices[2], leading to the observation of zero-field transport regimes dominated by either electron-electron[3], electron-hole[4] or electron-phonon (e-ph) interaction[5], which manifest over different carrier density and temperature ranges. Toward RT ($T \sim 300$ K), the scattering of electrons with acoustic phonons was theoretically identified as the main intrinsic contribution to the electrical resistivity in graphene[6–8], implying a carrier mobility exceeding 10^5 cm^{2}V^{-1}s^{-1} at low carrier concentration ($n < 10^{12}$ cm^{-2}). While such figures could already be inferred from early data on disordered SiO_2-supported graphene (~10^4 cm^{2}V^{-1}s^{-1} mobility)[9,10], at present, the reach of the zero-field acoustic-phonon-limit is firmly established as a generic property of high-quality graphene devices[5], also when encapsulated in hBN crystals from different sources[11] or engineered to high doping levels ($n > 10^{13}$ cm^{-2})[12]. Notable exceptions to the cleanness-implies-high-RT-

[1]Nanotechnology Group, USAL–Nanolab, Universidad de Salamanca, E-37008 Salamanca, Spain. [2]JARA-FIT and 2nd Institute of Physics, RWTH Aachen University, 52074 Aachen, Germany. [3]Peter Grünberg Institute (PGI-9), Forschungszentrum Jülich, 52425 Jülich, Germany. [4]CENTERA Laboratories, Institute of High Pressure Physics, Polish Academy of Sciences, 29/37 Sokołowska Str, Warsaw, Poland. [5]High Field Magnet Laboratory (HFML-EMFL), Radboud University, Toernooiveld 7, 6525 ED Nijmegen, The Netherlands. [6]Radboud University, Institute for Molecules and Materials, Heyendaalseweg 135, 6525 AJ Nijmegen, The Netherlands. [7]Research Center for Functional Materials, National Institute for Materials Science, 1-1 Namiki Tsukuba, Ibaraki 305-0044, Japan. [8]International Center for Materials Nanoarchitectonics, National Institute for Materials Science, 1-1 Namiki Tsukuba, Ibaraki 305-0044, Japan. [9]NEST, Istituto Nanoscienze-CNR and Scuola Normale Superiore, Piazza San Silvestro 12, 56127 Pisa, Italy. [10]These authors contributed equally: Daniel Vaquero, Vito Clericò. ✉e-mail: sergio.pezzini@nano.cnr.it

mobility scenario are suspended graphene samples, where flexural phonons dramatically contribute to carrier scattering leading to a T^2 behaviour of the resistivity[13], and rotationally faulted graphene bilayers close to magic-angle, showing strong phonon-driven T-linear resistivity[14]. The difference between freely suspended graphene and graphene encapsulated in hBN is due to the fact that in the latter case van der Waals interaction between graphene and substrate makes flexural phonons harder, suppressing an intrinsic rippling instability[15].

In this work, we address the fundamental question whether the e-ph mechanism in clean graphene could also govern the electrical transport in the QH regime[16] at temperatures close to RT. In this sense, we note that previous literature on the RT-QH effect in graphene[17–20] exclusively includes experiments on SiO_2-supported devices, precluding such investigation.

Results

The QH effect in 2DESs manifests when the Fermi level (E_F) lies on the localised states between two LLs, formed in a perpendicular magnetic field and separated by an energy gap Δ_{LL}. The interplay between this energy scale and the thermal energy kT governs the basic phenomenology of the electrical transport in the QH regime. When $kT \ll \Delta_{LL}$, no conduction takes place in the 2D bulk, while 1D chiral edge states carry the electrical current ballistically, leading to zero longitudinal resistivity (ρ_{xx}) when measured in four-probe configuration (Fig. 1a, upper panel). As the temperature increases and $kT \sim \Delta_{LL}$, thermal excitation of extended bulk states (close to the LLs centre) exponentially restores bulk conduction and carrier scattering (Fig. 1a, lower panel), resulting in a finite value of the longitudinal resistivity minimum according to $\rho_{xx} = \rho_0 \exp(-\Delta_{LL}/2kT)$. This relation is vastly employed to estimate the inter-LL separation via T-dependent measurements of the local resistivity minimum (under the precaution that the activation energy underestimates Δ_{LL} due to disorder-broadening of the LLs[21]).

The pre-factor to the exponential term, ρ_0, which is often not considered explicitly, determines the magnitude of the T-activated resistivity (shaded yellow area Fig. 1a, lower) and contains information regarding the disorder potential[22,23]. In perpendicular magnetic fields, e-ph scattering requires lattice vibrations with a wave-vector in the order of the inverse of the magnetic length ($l_B \sim 25\,\mathrm{nm}/\sqrt{B[\mathrm{T}]}$)[24], which defines a third energy scale relevant to our problem $E_{ph} = \hbar v_s / l_B$ (where v_s is the sound velocity in the material). In conventional 2DESs, the small Δ_{LL} leads to a complete suppression of the QH effect within a few K[25], where the E_{ph}-controlled phonon population can be considered negligible. Although the low electronic mass in 2DESs such as InSb[26] and HgTe[27–29] enables the observation of the QHE up to liquid-nitrogen temperature, this is insufficient to ensure $kT \gg E_{ph}$ and therefore insufficient to realize a predominance of e-ph interaction. This condition, as sketched in Fig. 1b, is instead fulfilled by graphene in the RT-QH regime (the field dependence of E_{ph} and the corresponding T-dependent excitation probability for acoustic phonons in graphene at $B = 30$ T are shown in Fig. S1). Under this circumstance, the T-activated resistivity (shaded dark cyan area in Fig. 1b) should directly relate to e-ph scattering[24].

Figure 1c shows a representative measurement of the RT-QH effect, acquired at $B = 30$ T in a hBN/graphene/hBN back-gated Hall bar (sample D2). The Hall conductivity (σ_{xy}) presents weak slope changes around filling factors $\nu = \pm 2$ ($V_g \sim \pm 20$ V), while the shelves-like features at low carrier concentration originate from the onset of electron-hole coexistence in the highly-degenerate $N = 0$ LL[30]. ρ_{xx}, in addition to the pronounced maximum around the charge neutrality point (CNP), shows two sizable minima (Fig. 1c, inset), indicative of T-activated QH states. Notably, the overall robustness of the RT-QH signatures dramatically differs in high-mobility graphene with respect to SiO_2-supported samples;[17] we thoroughly address this striking observation in a separate work, where we study the suppression of the σ_{xy} plateaus in

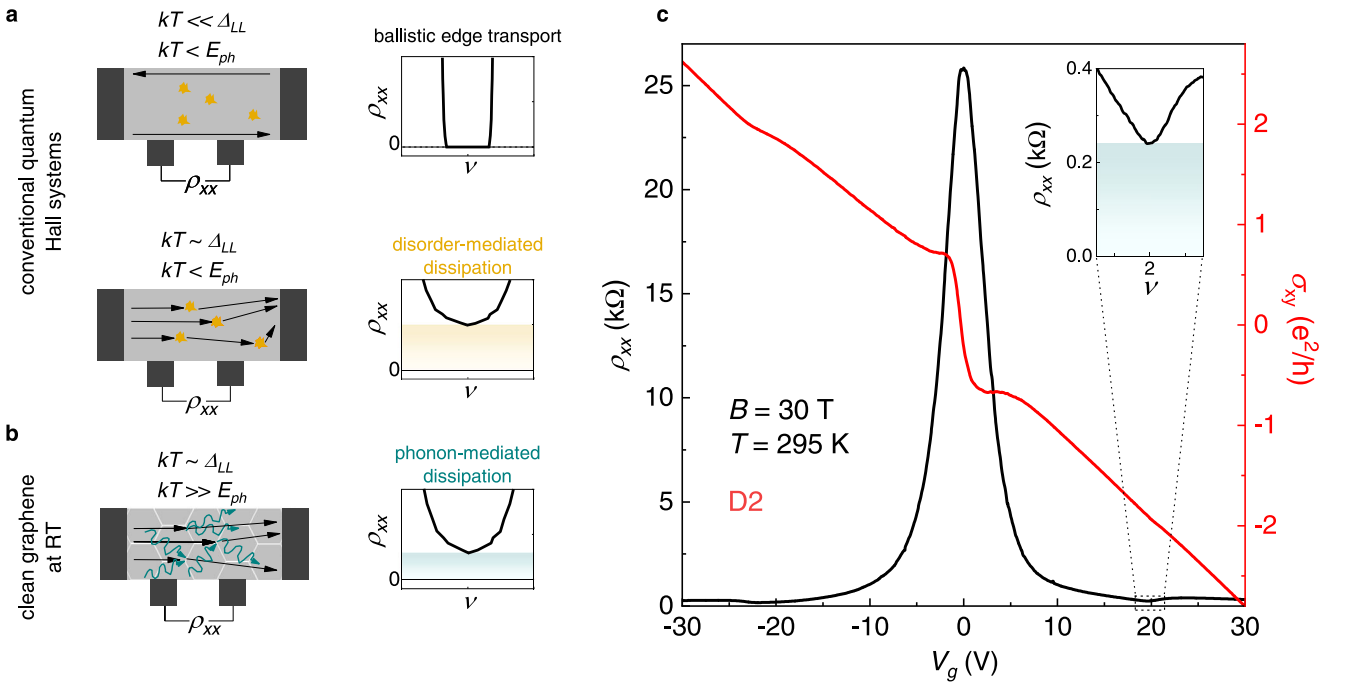

Fig. 1 | Dissipation regimes in the quantum Hall phase: high-quality graphene at RT. a Schematics of temperature-dependent transport in conventional quantum Hall systems, such as 2DESs in semiconductors. At low T (relative to the LL separation, upper part), the electrical current is carried by chiral edge states, leading to zero longitudinal resistance. At higher T (lower part), thermally-excited bulk states give a finite resistivity due to disorder scattering (yellow shading), with negligible contribution from lattice vibrations. **b** At RT, graphene supports both the QH effect (due to large inter-LL spacing) and predominant e-ph scattering in high-mobility samples, enabling the realization of a different transport regime, with phonon-mediated dissipation at high magnetic fields (dark cyan shading). **c** ρ_{xx} (black) and σ_{xy} (red) as a function of the back-gate voltage (corrected by a 5.2 V offset from the CNP), measured in hBN-encapsulated sample D2 at $B = 30$ T and $T = 295$ K. Inset: zoom-in of ρ_{xx} in the vicinity of filling factor $\nu = 2$ (the dark cyan shading indicates the finite value of the resistivity minimum).

https://doi.org/10.1038/s41467-023-35986-3

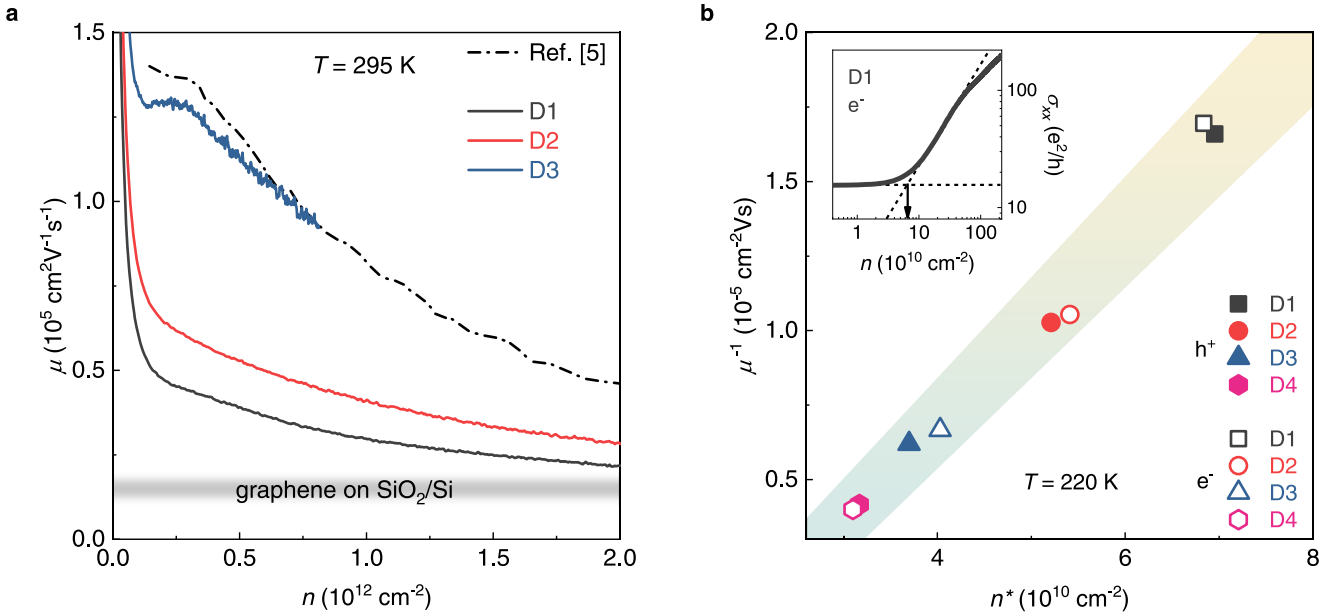

Fig. 2 | Phonon-limited transport and residual disorder at zero magnetic field. **a** RT carrier mobility (calculated according to the Drude model) as a function of the carrier concentration, for three hBN-encapsulated devices. The reference dash-dotted line are data from ref. [5], indicating a carrier mobility limited by electron-acoustic phonon scattering. The grey-shaded area shows the typical mobility for SiO_2-supported graphene devices, $1–2 \times 10^4$ $cm^2V^{-1}s^{-1}$. **b** Inverse of the high-temperature (220 K) field-effect mobility as a function of charge inhomogeneity n^*, for hBN/graphene/hBN devices D1-4. The shaded area covers a linear fit to the data, as in ref. [33], ± one standard error on the best-fit intercept and slope. Inset: Log-Log plot of the longitudinal conductivity of sample D1 as a function of the carrier density, exemplifying the extraction of n^* (black arrow).

ultra-high-quality devices at temperatures significantly lower than RT. In the following, we will focus on the magnitude of ρ_{xx} in the RT-QH regime and identify the underlying mechanism employing a collection of dry-assembled hBN/graphene/hBN heterostructures.

In Fig. 2 we present the main transport characteristics of our devices (details on the fabrication are given in Methods), measured at zero magnetic field and at elevated temperatures. Figure 2a shows the RT mobility of three hBN-encapsulated devices, calculated according to the Drude model ($\mu = 1/(ne\rho_{xx})$), as a function of the carrier density n. All the mobility curves are well above the typical values for SiO_2-supported graphene (grey shaded area) over the whole n range. Importantly, sample D3 shows a $\mu(n)$ dependence comparable to the data of ref. [5] (dash-dotted line), demonstrating the standard fingerprint of phonon-limited RT mobility in zero magnetic field[11,12] (as confirmed by temperature-dependent resistivity data shown in Fig. S2). We note that, although Wang et al. employed a 15 μm-wide van der Pauw device, e-ph scattering imposes a ~1 μm upper bound to the electronic mean free path at $B = 0$ and RT[5]. Therefore, the zero-field e-ph limit can also be realized using narrow Hall bars, provided that their channel width exceeds 1 μm (1.5 μm to 2.3 μm in our devices). The overall high quality of the samples is also supported by the observation of fractional QH states at liquid-helium temperature (see data for sample D2 in Fig. S3, and ref. [31] for sample D4, fabricated using CVD-grown graphene). In Fig. 2b we explore the correlation between the carrier mobility (calculated using the field-effect formula[32]) and the charge inhomogeneity in the CNP region, estimated as the usual n^* parameter[33] (see Fig. 2b inset for an example of the extraction). We consider data at $T = 220$ K, where clear thermal activation is observed in the RT-QH regime. n^* values above the intrinsic CNP thermal broadening (~2.6×10^{10} cm^{-2} at 220 K, beginning of the x-axis in Fig. 2b) quantify the residual disorder, which, in our devices, remains well below the typical observations for graphene on SiO_2 (n^* in the few-10^{11} cm^{-2} range). In addition, as for refs. [33,34], the linear $\mu^{-1}(n^*)$ dependence (see shaded area in Fig. 2b) indicates scattering from long-range potentials, attributed to random strain variations generic to graphene on substrates[35]. We can therefore conclude that the devices at disposal (i) span a low-disorder range unexplored in previous RT-QH experiments, and (ii) present a well-defined disorder type, with increasing impact along the D4-to-D1 sequence.

We then employ the sample temperature as an experimental knob to control the excitation of both phonons (see Fig. S1) and bulk-extended electronic states in strong magnetic fields. In Fig. 3a we sketch the effect of increasing T on the Landau-quantized electrons in graphene at $B = 30$ T. Toward RT, the broadening of the Fermi-Dirac distribution around E_F (experimentally set by V_g) ensures excited charge carriers from both the $N = 0$ and $N = 1$ LLs, across the giant gap Δ_{LL}. Accordingly, the local resistivity minimum at filling factor $\nu = 2$ leaves zero and displays increasing finite values, as shown in the experimental curves of Fig. 3b. In Fig. 3c, we present a complete picture of the T-dependence of ρ_{xx} ($\nu = 2$) for samples D1-4, at selected magnetic fields (30 T and 25 T in the main panel and inset, respectively; data at $\nu = -2$ are shown in Fig. S4). In addition to our data, we show reference points from ref. [20] (black diamonds, ρ_{xx} ($\nu = 2$) in graphene on SiO_2), and two theoretical calculations defining different dissipation limits (continuous lines). In both cases we take an activation energy equal to $\Delta_{LL}/2$: this was shown to be accurate for high B-fields in ref. [20] and should hold true for clean graphene with reduced LL broadening. The upper line (yellow) assumes the universal conductivity pre-factor due to long-range disorder ($2e^2/h$)[23], multiplied by a factor 4 to take into account the LL degeneracy of graphene. The lower line (dark cyan) is based on the work by Alexeev et al.[24], who calculated the conductivity mediated by two-phonon scattering for graphene in the RT-QH regime. The relevant e-ph process conserves the LL number, but modifies the in-plane electronic momentum. We note that this phenomenology is fundamentally different from that of magnetophonon oscillations, recently discovered in extra-wide graphene devices[36], which rely on resonant inter-LL scattering at $T < 200$ K. Here, two-phonon scattering within each LL contributes with a conductivity pre-factor $\sigma_0 = \sigma_N(T/300\,\mathrm{K})(B/10\,\mathrm{T})^{1/2}$, which depends both on temperature and magnetic field (in contrast to the constant pre-factor commonly

https://doi.org/10.1038/s41467-023-35986-3

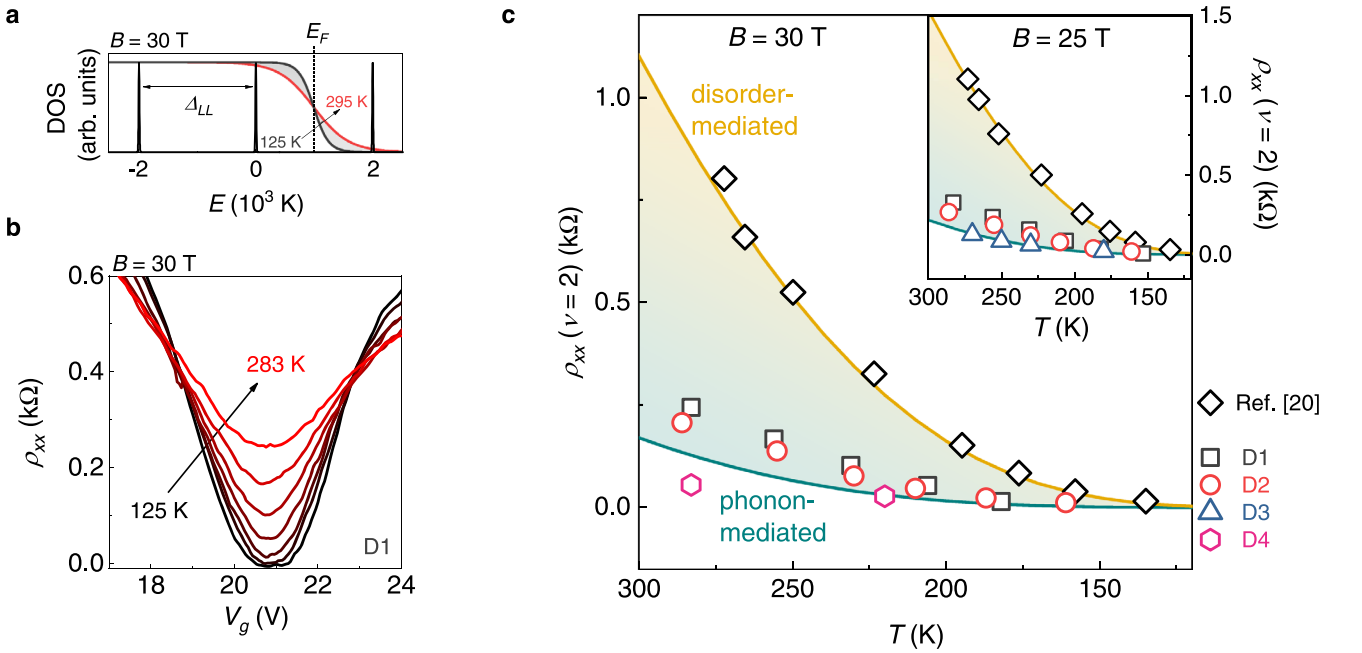

Fig. 3 | Temperature-activated resistivity and phonon-mediated dissipation in the quantum Hall effect. a Density of states (DOS) of graphene as a function of energy, at $B = 30$ T (with a realistic value of LL broadening of 15 K). On top of the DOS we show the Fermi-Dirac distribution, with E_F positioned in the middle of the $N = 0$ and $N = 1$ LL, at two different temperatures, representative of the experimental range considered. **b** Temperature-activated longitudinal resistivity in the vicinity of $\nu = 2$, measured in sample D1. **c** Minimum of ρ_{xx} at $\nu = 2$ as a function of temperature, for the hBN-encapsulated devices. The reference data (black diamonds) are from ref. [20]. The yellow and dark cyan continuous line are theoretical calculations based on refs. [23,24], respectively (the shading covers resistivity values within the two theoretical calculations). The magnetic field is 30 T (25 T) in the main panel (inset).

assumed in QH studies). In the $\nu = 2$ state, the predominant contribution to the σ_N terms comes from the $N = 0$ LL (0.65 e^2/h, one order of magnitude larger with respect to $N = 1$, 0.06 e^2/h)[24]. Strikingly, the resulting activated behaviour, not including any free parameter, is well approximated by our devices, while the reference data from graphene on SiO_2 follow the long-range disorder limit. The qualitative agreement between theoretical calculations and experimental data, together with the contrasting behaviour with respect to previous reports[20], indicate that graphene/hBN heterostructures support an e-ph-dominated transport in the RT-QH regime. Arrhenius-type fits to the conductivity[37], shown in Fig.S5, confirm the contrasting magnitude of the pre-factor for the two generations of graphene devices (as well as the correctness of the assumed gap size).

Despite the presence of long-range potentials (Fig. 2b), our data clearly indicate that the e-ph pre-factor does not simply add up to the standard long-range disorder term. To elucidate this point, we quantitatively analyse the deviation from the phonon-mediated limit in the different devices. We proceed by fitting the data from samples D1-3 (only two high T curves are acquired for D4 due to experimental limitations) with a generalized relation (Fig. 4, inset), which adds to the theoretical e-ph dependence from ref. [24] an activation part with a constant pre-factor (ρ_D). This term is intended to account for the effect of residual disorder, and it is the only free parameter in the fits. In Fig. 4 we plot the extracted ρ_D for the three samples at different magnetic fields, as a function of the n^* parameter (averaged between the electron and hole-side). The linear $\rho_D(n^*)$ behaviour observed here (shaded area in Fig. 4) indicates that the random strain variations inducing the CNP broadening are also responsible for ρ_{xx} exceeding the e-ph limit in the RT-QH regime. Notably, the only device to display an exact e-ph-type dependence (D3, $\rho_D \sim 0$), is also the one to show a Drude mobility comparable to the zero-field e-ph limit[5]. Taking into account the sample-dependent correction due to residual disorder, in SI (Fig. S6) we proceed to a quantitative investigation of the field and temperature dependence of the conductivity pre-factor in our samples, revealing

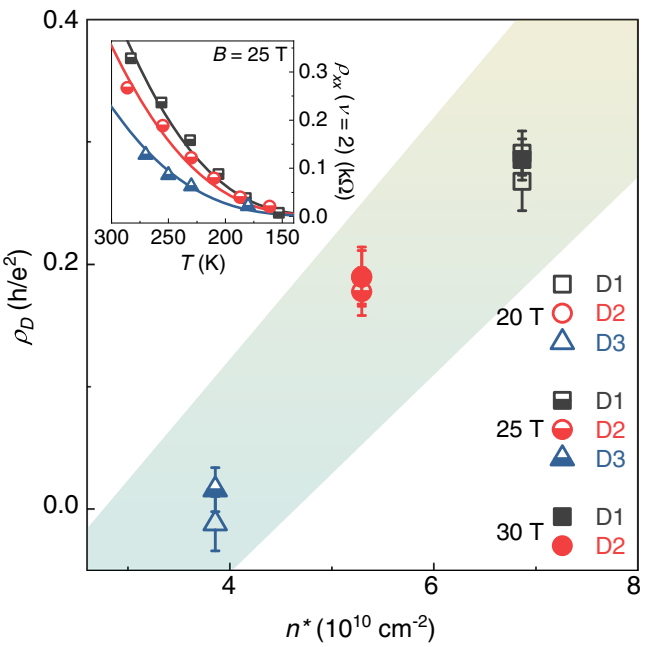

Fig. 4 | Sample-dependent disorder contribution to the activated resistivity. Correlation between the T-independent pre-factor to the activated resistivity and n^*(220 K) for devices D1-3. The shaded area is defined as in Fig. 2b. The error bars correspond to ± one standard error from the fits shown in the inset. Inset: fits to the minimum resistivity as a function of temperature (continuous lines), using the generalized formula including both e-ph and disorder contributions, at $B = 25$ T.

the expected $B^{1/2}$ behaviour of the e-ph term. However, we note that the simplified pre-factor proposed in ref. [24] is the result of several approximations and, more importantly, it neglects the effect of disorder. To better understand the interplay between the different

scattering mechanisms underlying the activated resistivity, in SI (Figs. S7 and S8) we discuss additional data at lower temperature (down to 50 K) and magnetic field (down to 1 T). We find that ρ_D drastically increases toward low T, with the activated resistivity exceeding the e-ph limit by more than one order of magnitude in a clean sample. However, as the temperature and magnetic field are increased, ρ_D progressively drops (i.e., the activated resistivity tends toward the e-ph limit), suggesting a temperature-driven crossover between regimes dominated by either disorder or e-ph interaction (the latter being realized only close to RT). While it is not surprising that the e-ph limit works as a lower bound to the activated resistivity of real samples, the non-universality (i.e., the sample and temperature dependence) of the disorder contribution deserves particular attention in future theoretical treatments of the RT-QH in graphene.

Discussion

The physics of graphene is essentially determined by its deviations from flatness (that is, ripples), due to either thermal fluctuations associated to flexural phonons for freely suspended samples or to roughness of substrate like for graphene on SiO_2[15]. In both cases, ripples induce inhomogeneity of electron density with electron and hole puddles in the vicinity of the CNP[38,39]. In particular, for the case of graphene on SiO_2 the amplitude of induced inhomogeneity of charge-carrier density is estimated as $3 \times 10^{11}\,cm^{-2}$[39], in agreement with the above cited experimental values of n^*. This makes the system strongly disordered, and any intrinsic scattering mechanisms become irrelevant. Oppositely, the hBN substrate is atomically flat[1] and at the same time suppresses intrinsic ripples which increases the RT carrier mobility by an order of magnitude and makes intrinsic scattering mechanisms dominant[15]. Indeed, experimentally measured n^* for our samples is an order-of-magnitude smaller than what is supposed to be induced by ripples at RT. This results in an essentially different picture of QH physics at high enough temperatures.

In conclusion, we showed experimental evidence of predominant e-ph scattering in the QH regime. This is realized by uniquely combining strong magnetic fields, high temperatures and hBN-encapsulation of graphene. Although the RT-QH in graphene has long been known, we showed that mitigation of disorder via van der Waals engineering provides novel insights on the transport mechanisms in this phenomenon.

Methods

Graphene-hBN van der Waals assembly and device fabrication

hBN/graphene/hBN samples D1-3 are assembled using the standard van der Waals dry pick-up[5], starting from micromechanically exfoliated graphene flakes previously identified by optical and Raman microscopy. Sample D4 is obtained by CVD growth on Cu foil and direct hBN-mediated pick-up after controlled decoupling via Cu surface oxidation[31]. All the devices are fabricated making use of electron beam lithography, reactive ion etching and e-beam evaporation of Cr/Au 1D edge contacts[5].

Magnetotransport measurements

We use standard lock-in acquisition at low frequency (13 Hz), with simultaneous ρ_{xx} and ρ_{xy} measurements in four-probe configuration, either under a constant current excitation (12.5 nA, sample D1-D3) or a constant voltage bias (300 μV, sample D4). The devices are mounted in a VTI system with low-pressure ^{4}He serving as exchange gas, coupling the samples to a liquid-N_2 reservoir. The cryogenic system is accommodated in the access bore of a resistive Bitter magnet at HFML-EMFL, with a maximum field of 33 T.

Reporting summary

Further information on research design is available in the Nature Portfolio Reporting Summary linked to this article.

Data availability

The data presented in this study are available at https://doi.org/10.5281/zenodo.7352031.

References

1. Yankowitz, M., Ma, Q., Jarillo-Herrero, P. & LeRoy, B. J. van der Waals heterostructures combining graphene and hexagonal boron nitride. *Nat. Rev. Phys.* **1**, 112–125 (2019).
2. Rhodes, D., Chae, S. H., Ribeiro-Palau, R. & Hone, J. Disorder in van der Waals heterostructures of 2D materials. *Nat. Mater.* **18**, 541–549 (2019).
3. Bandurin, D. A. et al. Negative local resistance caused by viscous electron backflow in graphene. *Science* **351**, 1055–1058 (2016).
4. Crossno, J. et al. Observation of the Dirac fluid and the breakdown of the Wiedemann–Franz law in graphene. *Science* **351**, 1058–1061 (2016).
5. Wang, L. et al. One-dimensional electrical contact to a two-dimensional material. *Science* **342**, 614–617 (2013).
6. Hwang, E. H. & Das Sarma, S. Acoustic phonon scattering limited carrier mobility in two-dimensional extrinsic graphene. *Phys. Rev. B* **77**, 115449 (2008).
7. Sohier, T. et al. Phonon-limited resistivity of graphene by first-principles calculations: Electron-phonon interactions, strain-induced gauge field, and Boltzmann equation. *Phys. Rev. B* **90**, 125414 (2014).
8. Park, C.-H. et al. Electron–phonon interactions and the intrinsic electrical resistivity of graphene. *Nano Lett.* **14**, 1113–1119 (2014).
9. Morozov, S. V. et al. Giant intrinsic carrier mobilities in graphene and its bilayer. *Phys. Rev. Lett.* **100**, 016602 (2007).
10. Chen, J.-H., Jang, C., Xiao, S., Ishigami, M. & Fuhrer, M. S. Intrinsic and extrinsic performance limits of graphene devices on SiO_2. *Nat. Nanotechnol.* **3**, 206 (2008).
11. Sonntag, J. et al. Excellent electronic transport in heterostructures of graphene and monoisotopic boron-nitride grown at atmospheric pressure. *2D Mater.* **7**, 031009 (2020).
12. Shi, W. et al. Reversible writing of high-mobility and high-carrier-density doping patterns in two-dimensional van der Waals heterostructures. *Nat. Electron.* **3**, 99–105 (2020).
13. Castro, E. V. et al. Limits on charge carrier mobility in suspended graphene due to flexural phonons. *Phys. Rev. Lett.* **105**, 266601 (2010).
14. Polshyn, H. et al. Large linear-in-temperature resistivity in twisted bilayer graphene. *Nat. Phys.* **15**, 1011–1016 (2019).
15. Katsnelson, M. I. *The Physics of Graphene*, 2nd ed. (Cambridge University Press, 2020).
16. Klitzing, K., Dorda, G. & Pepper, M. New method for high-accuracy determination of the fine-structure constant based on quantized hall resistance. *Phys. Rev. Lett.* **45**, 494 (1980). v.
17. Novoselov, K. S. et al. Room-temperature quantum hall effect in graphene. *Science* **315**, 1379 (2007).
18. Jiang, Z., Zhang, Y., Tan, Y.-W., Stormer, H. L. & Kim, P. Quantum hall effect in graphene. *Solid State Commun.* **143**, 14–19 (2007).
19. Jiang, Z., Zhang, Y., Tan, Y.-W., Stormer, H. L. & Kim, P. Quantum hall states near the charge-neutral dirac point in graphene. *Phys. Rev. Lett.* **99**, 106802 (2007).
20. Giesbers, A. J. M. et al. Quantum-hall activation gaps in graphene. *Phys. Rev. Lett.* **99**, 206803 (2007).
21. Ando, T., Fowler, A. B. & Stern, F. Electronic properties of two-dimensional systems. *Rev. Mod. Phys.* **54**, 437 (1982).
22. Polyakov, D. G. & Shklovskii, B. I. Activated conductivity in the quantum hall effect. *Phys. Rev. Lett.* **73**, 1150 (1994).
23. Polyakov, D. G. & Shklovskii, B. I. Universal prefactor of activated conductivity in the quantum hall effect. *Phys. Rev. Lett.* **74**, 150 (1995).

24. Alexeev, A. M., Hartmann, R. R. & Portnoi, M. E. Two-phonon scattering in graphene in the quantum Hall regime. *Phys. Rev. B* **92**, 195431 (2015).
25. Das Sarma, S. & Pinczuk, A. *Perspectives in Quantum Hall Effects* (Wiley, New York, 1997).
26. Murphy, S. Q. et al. Studies of the quantum Hall to quantum Hall insulator transition in InSb-based 2DESs. *Phys. E* **6**, 293 (2000).
27. Landwehr, G. et al. Quantum transport in n-type and p-type modulation-doped mercury telluride quantum wells. *Phys. E* **6**, 713 (2000).
28. Kozlov, D. A. et al. Quantum Hall effect in HgTe quantum wells at nitrogen temperatures. *Appl. Phys. Lett.* **105**, 132102 (2014).
29. Khouri, T. et al. High-temperature quantum Hall effect in finite gapped HgTe quantum wells. *Phys. Rev. B* **93**, 125308 (2016).
30. Wiedmann, S. et al. Coexistence of electron and hole transport in graphene. *Phys. Rev. B* **84**, 115314 (2011).
31. Schmitz, M. et al. Fractional quantum Hall effect in CVD-grown graphene. *2D Mater.* **7**, 041007 (2020).
32. Kim, S. et al. Realization of a high mobility dual-gated graphene field-effect transistor with Al_2O_3 dielectric. *Appl. Phys. Lett.* **94**, 062107 (2009).
33. Couto, N. J. G. et al. Random strain fluctuations as dominant disorder source for high-quality on-substrate graphene devices. *Phys. Rev. X* **4**, 041019 (2014).
34. Wang, L. P. et al. Mobility enhancement in graphene by in situ reduction of random strain fluctuations. *Phys. Rev. Lett.* **124**, 157701 (2020).
35. Neumann, C. et al. Raman spectroscopy as probe of nanometer-scale strain variations in graphene. *Nat. Commun.* **6**, 8429 (2015).
36. Kumaravadivel, P. et al. Strong magnetophonon oscillations in extra-large graphene. *Nat. Commun.* **10**, 3334 (2019).
37. Usher, A. et al. Observation of magnetic excitons and spin waves in activation studies of a two-dimensional electron gas. *Phys. Rev. B* **41**, 1129 (1990).
38. Gibertini, M., Tomadin, A., Polini, M., Fasolino, A. & Katsnelson, M. I. Electron density distribution and screening in rippled graphene sheets. *Phys. Rev. B* **81**, 125437 (2010).
39. Gibertini, M., Tomadin, A., Guinea, F., Katsnelson, M. I. & Polini, M. Electron-hole puddles in the absence of charge impurities. *Phys. Rev. B* **85**, 201405 (2012).

Acknowledgements

We acknowledge technical support from Y. Lechaux and J. Quereda. This work has been supported by Ministerio de Ciencia e Innovación (Grant PID2019-106820RB-C2-2) and Junta de Castilla y León (Grants SA256P18 and SA121P20, including EU/FEDER funds). This work was supported by HFML-RU/NWO-I, member of the European Magnetic Field Laboratory (EMFL). This work was also supported by CENTERA Laboratories in the frame of the International Research Agendas Program for the Foundation for Polish Sciences co-financed by the European Union under the European Regional Development Fund (no. MAB/2018/9). D.V. acknowledges financial support from the Ministry of Universities (Spain) (Ph.D. contract FPU19/04224). J.A.D-N thanks the support from the Universidad de Salamanca for the María Zambrano postdoctoral grant funded by the Next Generation EU Funding for the Requalification of the Spanish University System 2021–23, Spanish Ministry of Universities. K.W. and T.T. acknowledge support from the Elemental Strategy Initiative conducted by the MEXT, Japan (Grant Number JPMXP0112101001) and JSPS KAKENHI (Grant Numbers 19H05790, 20H00354 and 21H05233).

Author contributions

U.Z., S.W. and S.P. conceived the experiment and coordinated the collaboration. D.V., V.C. and M.S. fabricated the graphene devices and performed the transport measurements. J.A.D.-N., A.M.-R. and J.S.-S. provided technical assistance in the cleanroom processing. C.S.A.M. and K.R. provided technical assistance during the high-field experiments. K.W. and T.T. provided single crystals of hBN. B.B., C.S. and E.D. supervised the experimental work. D.V., V.C., M.S., and S.P. performed the data analysis. M.I.K. provided theoretical input for the interpretation of the results. S.P. wrote the manuscript with input from all the co-authors.

Competing interests

The authors declare no competing interests.

Additional information

Supplementary information The online version contains supplementary material available at https://doi.org/10.1038/s41467-023-35986-3.

Correspondence and requests for materials should be addressed to Sergio Pezzini.

Peer review information *Nature Communications* thanks Mikhail Portnoi and the anonymous reviewers for their contribution to the peer review of this work.